Nuclear Instruments and Methods in Physics Research A 604 (2009) 618–623

Contents lists available at ScienceDirect

Nuclear Instruments and Methods in Physics Research A

journal homepage: www.elsevier.com/locate/nima

Neutron and gamma-ray cross-correlation measurements of plutonium oxide powder

S.D. Clarke [a,*], M. Flaska [a], S.A. Pozzi [a], P. Peerani [b]

[a] Department of Nuclear Engineering & Radiological Sciences, University of Michigan, 2328B Cooley Building, 2355 Bonisteel Blvd., Ann Arbor, MI 48109, USA
[b] European Commission EC-JRC-IPSC, Ispra, Italy

ARTICLE INFO

Article history:
Received 11 December 2008
Received in revised form
17 February 2009
Accepted 26 February 2009
Available online 5 April 2009

Keywords:
Cross-correlation
Plutonium oxide
Special nuclear material
Liquid scintillator
MCNP-PoliMi

ABSTRACT

For the first time, measurements of the time-dependent cross-correlation distributions of plutonium oxide have been made separately for neutrons and gamma rays. Six EJ-309 liquid scintillation detectors with a digital, offline pulse shape discrimination and pulse timing method were used to measure five different samples of varying mass and burnup. The number of (neutron, neutron) correlations were selectively analyzed versus plutonium mass and a clear, increasing trend was observed. Additionally, the measurement scenarios were modeled using the MCNP-PoliMi code and good agreement was observed between the measured and simulated cross-correlation functions.

1. Introduction

Neutron and gamma-ray measurements using organic scintillation detectors are widely applied in fields such as nuclear nonproliferation, international safeguards, nuclear material control and accountability, and national security. In contrast to thermal neutron detectors such as ^{3}He tubes, organic scintillators are able to detect high-energy neutrons without use of moderating material. At the same time, these detectors are sensitive to gamma rays, which makes them very suitable for measurements in mixed neutron/gamma-ray fields.

Previous measurements on plutonium oxide (PuO_2) samples that are stored at the Performance Laboratory of the Joint Research Centre (JRC) in Ispra were performed in 2004 and 2005 and included the measurement of the total neutron and gamma-ray cross-correlation functions [1]. The new measurements presented in this paper were performed jointly by the University of Michigan and JRC staff. In these measurements, time-dependent cross-correlation distributions were measured separately for neutron and gamma-ray events for the first time. The (neutron, neutron) portion of the cross-correlation function consists mainly of spontaneous fission neutrons from the even-numbered plutonium isotopes (reactions such as (α, n) produce single neutrons and several gamma rays). This selective analysis of (neutron, neutron) correlated counts provides information related to the mass of the plutonium in the sample.

2. Measurement technique

2.1. Description of measurement setup

The PuO_2 powder is stored in cylindrical steel containers with various heights and diameters and with a mass between 50 and 500 g. The measurement setup consisted of six cylindrical, EJ-309 liquid scintillation detectors (13.3 cm high and 13 cm in diameter) placed symmetrically around the sample at a distance of approximately 30 cm. Lead shielding sleeves with a total thickness of approximately 2.6 cm were placed around each sample to reduce the gamma-ray background. Fig. 1 shows a photograph of the measurement setup: all six EJ-309 scintillators and the centrally located sample holder are shown.

A CAEN V1720, 12-bit, 250-MHz digitizer was used to sample and store pulses directly from the anodes of the detectors. Six of the eight available channels were used for these measurements, the timing of which is synchronized by the digitizer board. A 100-keVee detection threshold was applied (this corresponds to a neutron energy of approximately 600 keV). Measurements were performed on five different samples of varying mass and burnup: 100-, 300-, and 500-g low-burnup samples and 50- and 100-g high-burnup samples. Table 1 lists the isotopic composition of the plutonium in the low- and high-burnup samples [2].

* Corresponding author. Tel.: +1 734 615 7830; fax: +1 734 763 4540.
E-mail address: clarkesd@umich.edu (S.D. Clarke).

0168-9002/$ - see front matter © 2009 Elsevier B.V. All rights reserved.
doi:10.1016/j.nima.2009.02.045

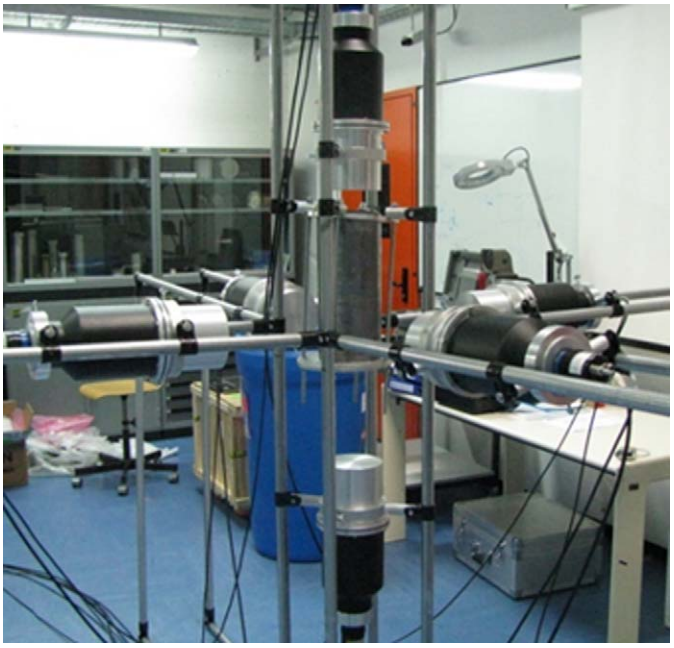

Fig. 1. Photograph of the measurement setup. Six EJ-309 liquid scintillators surround the centrally located sample inside of the lead shielding sleeves.

Table 1
Isotopic composition (mass percent) of low- and high-burnup PuO_2 samples.

Isotope	Low burnup (%)	High burnup (%)
^{238}Pu	0.20	1.72
^{239}Pu	70.96	58.10
^{240}Pu	24.58	24.77
^{241}Pu	3.29	9.77
^{242}Pu	0.98	5.65

2.2. Digital pulse shape discrimination and pulse timing

To distinguish neutrons from gamma rays, an offline digital PSD method was used [3]. This method is based on a standard charge integration method [4,5] that calculates the integral ratio of two different pulse intervals. The first interval covers the tail of a pulse, while the second interval covers the total pulse. Fig. 2 shows an illustration of a typical light pulse shape and these two integration regions where T_{1start} is the starting time for the total integral (A_1), T_{2start} is the starting time for the tail integral (A_2), and T_{end} is the ending time for both integrals. The parameters T_{2start} and T_{end} should be optimized for the specific detector system. In these measurements, the values were chosen to be $T_{2start} = 20$ ns and $T_{end} = 220$ ns for optimum separation based on past experience with these detector types [3].

Generally, heavier particles produce pulses with a larger fraction of light in the tail. This results in a larger ratio of tail-to-total integrals for neutrons when compared to gamma rays [6,7].

$$R \equiv \frac{\text{Tail integral}}{\text{Total integral}} = \frac{A_2}{A_1} \quad (1)$$

Pulse timing was achieved by measuring the time at which the pulse reaches 20% of the pulse amplitude, as shown in Fig. 2. Timing is performed by linear interpolation between two adjacent measured pulse samples. In this way, the inherent 4-ns resolution

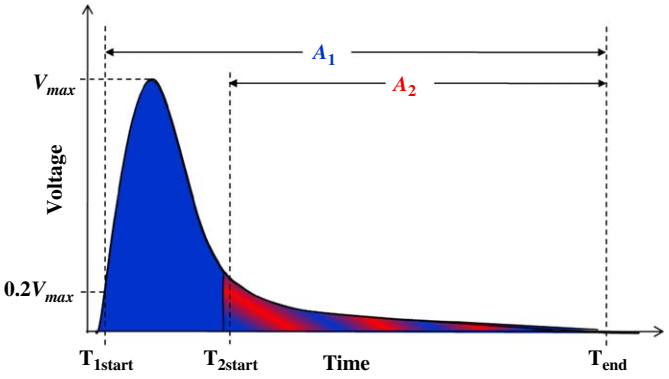

Fig. 2. Illustration of the pulse shape obtained from the EJ-309 liquid scintillator. The total integral (A_1) and tail integral (A_2) are computed for each pulse and used for classification as a neutron or gamma ray. Pulse timing was achieved by measuring the time at which the pulse reaches 20% of the pulse amplitude.

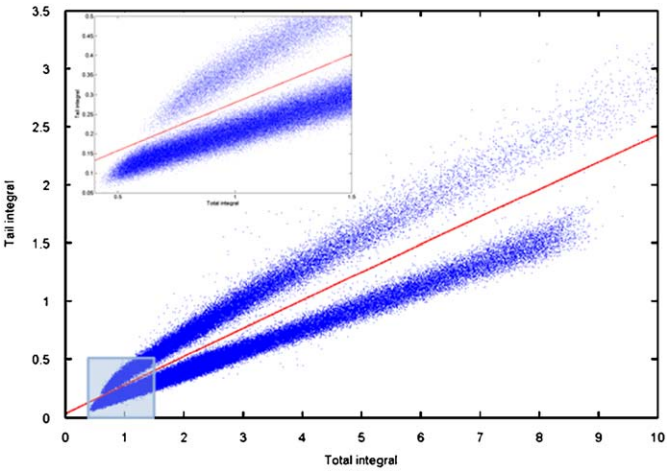

Fig. 3. Tail and total pulse integrals for measured pulses from a 500-g, low-burnup PuO_2 sample. The discrimination line is shown: pulses above the line are classified as neutrons and below the line as gamma rays. The low-energy region is shown in the inset.

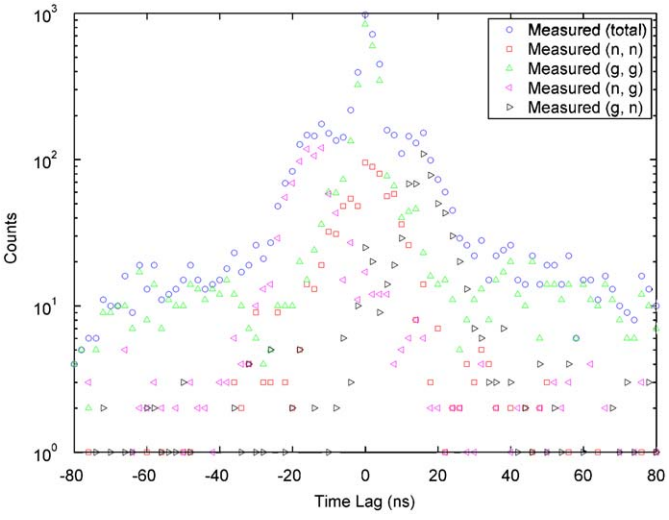

Fig. 4. Measured cross-correlation functions for a 100-g sample of low-burnup PuO_2 powder. Separate contributions are also shown ("n" stands for neutron, "g" stands for gamma ray).

of the digitizer is improved to approximately 1-ns resolution. The average time resolution is approximately equal to the full-width at half-maximum values of the gamma–gamma correlation curve, which was observed to be 4 ns. Cross-correlation functions were calculated by determining the time difference between detections in two separate detectors within a given time window.

3. Measurement results

Fig. 3 shows the tail and total integrals for 200,000 pulses collected from a single EJ-309 scintillator. The discrimination line is also shown: pulses above this line are classified as neutrons and below this line as gamma rays. The inset of the figures shows a zoom of the low-energy region of the plot. Very good separation of neutrons and gamma rays is observed even for these small pulses close to the measurement threshold of 100 keVee.

Fig. 4 shows measured cross-correlation functions for the 100-g, low-burnup PuO_2 sample (Figs. 5 and 6 show the results for the 300- and 500-g samples). The cross-correlation distributions were obtained by summing the signals from all pairs of detectors placed at 90° with respect to each other. The four main features of the total cross-correlation function are the two central and two side peaks; the first central peak occurs at time zero as a result of two fission gamma rays arriving in coincidence at the detectors (g–g pairs). The second central peak occurs around time zero as a result of two fission neutrons detected in coincidence (n–n pairs). The side peaks are a consequence of a fission neutron arriving in coincidence with a gamma ray (g–n and n–g pairs). Because the neutron velocity depends on the neutron energy, and is always smaller in magnitude than the gamma-ray velocity, the gamma–neutron, neutron–gamma, and neutron–neutron peaks are broader than the gamma–gamma peak. The gamma–neutron and neutron–gamma peaks occur at an absolute time different than time zero.

Fig. 7 shows the measured cross-correlation functions for the 50-g, high-burnup PuO_2 sample (Fig. 8 shows the results for the 100-g sample). All of the bulk features are similar to the results shown in Figs. 4–6. However, there are a few major differences due to the higher sample burnup. The most noticeable difference

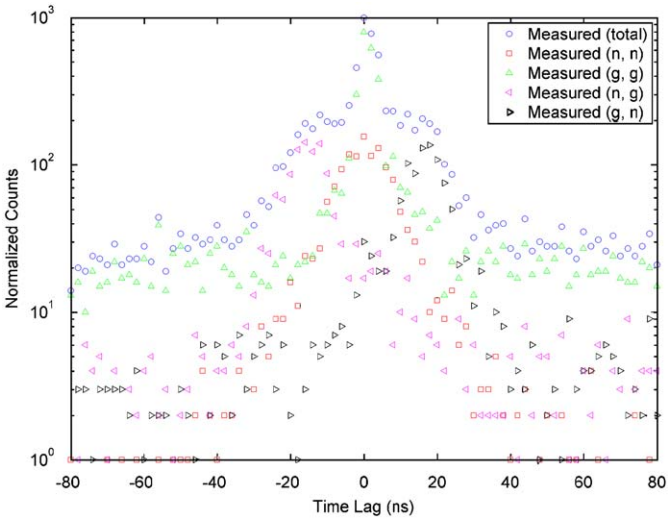

Fig. 5. Measured cross-correlation functions for a 300-g sample of low-burnup PuO_2 powder. Separate contributions are also shown (“n” stands for neutron, “g” stands for gamma ray).

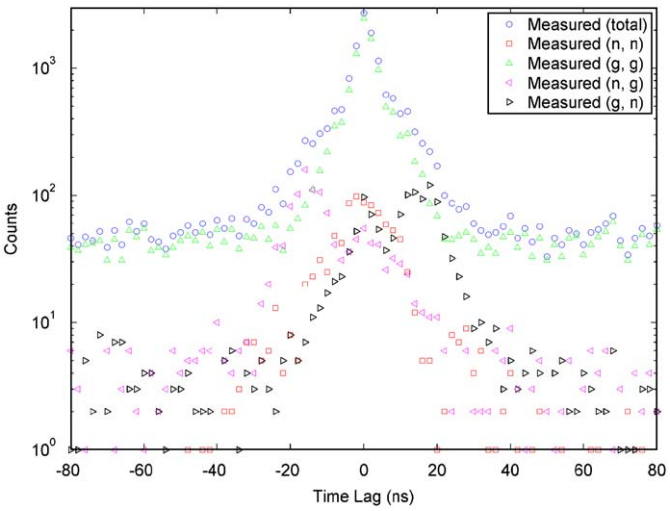

Fig. 7. Measured cross-correlation functions for a 50-g sample of high-burnup PuO_2 powder. Separate contributions are also shown (“n” stands for neutron, “g” stands for gamma ray).

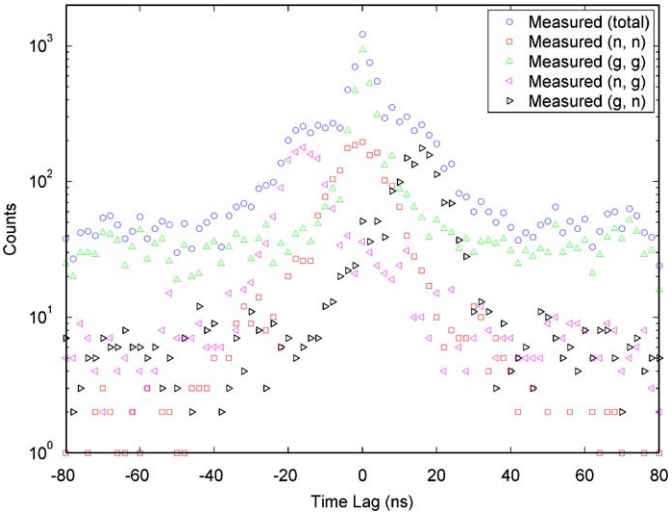

Fig. 6. Measured cross-correlation functions for a 500-g sample of low-burnup PuO_2 powder. Separate contributions are also shown (“n” stands for neutron, “g” stands for gamma ray).

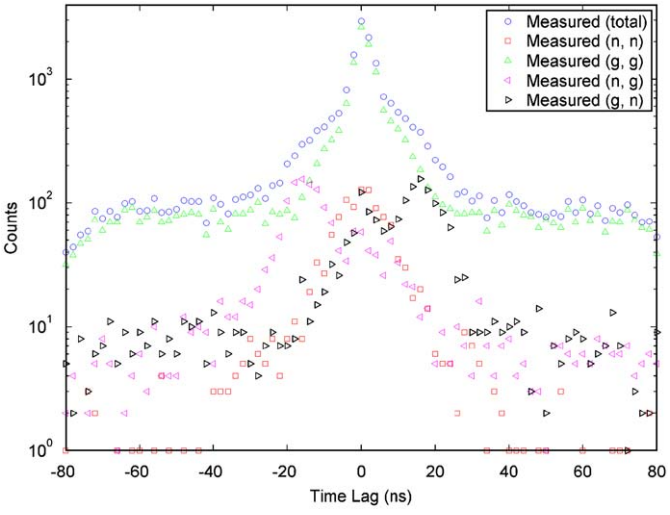

Fig. 8. Measured cross-correlation functions for a 100-g sample of high-burnup PuO_2 powder. Separate contributions are also shown (“n” stands for neutron, “g” stands for gamma ray).

Table 2
Total number of measured correlations and accidentals for each sample.

Burnup	Sample mass (g)	Net mass (g)	Total correlations	Calculated accidentals	Ratio of accidentals to total correlations
Low	100	98.089	5976±77	1138±34	0.190±0.006
	300	298.089	8205±91	2335±48	0.285±0.007
	500	501.984	11107±105	3868±62	0.348±0.006
High	50	51.455	16947±130	4246±65	0.251±0.004
	100	100.456	21081±145	7209±85	0.342±0.005

The ratio of the accidentals to the total number of measured correlations is also shown.

is the much larger level of accidental coincidences relative to the other portions of the distribution. The increased sample burnup results in greater fission product and ^{241}Am buildup providing a higher level of background. This fact leads to the second major difference: the (gamma, gamma) portion of the distribution is much larger than that of the low-burnup distributions. The data in Figs. 4–8 are un-normalized and were collected for varying acquisition times dependent upon laboratory conditions. As such, the relative magnitude of each curve is not indicative of the relative source strengths.

The coincident detections can be real or accidental in nature. Real coincidences occur when multiple particles are detected that originate from the same reaction. Accidental coincidences occur when two particles are detected in the coincident window, but are not from the same reaction. Particles in these measurements originate primarily from three reactions: spontaneous and induced fission, (α, n) on oxygen, and gamma-ray decay. Because fission is the only reaction of the three to emit multiple neutrons, the majority of (n, n) coincidences can be attributed to fission with a small fraction of accidentals. Gamma–gamma coincidences can arise from fission as well, but they may also be due to multiple decay gamma rays. Gamma–neutron (and neutron–gamma) coincidences arise from both fission and (α, n) reactions on oxygen.

Accidental coincidence rates are proportional to the size of the measurement gate window. For this kind of fast coincidence method, the coincidence gate can be kept very short (typically 50 ns), which constitutes the major advantage of this method over all classical techniques based on thermal neutron detection, where the gate is of the range of tens of microseconds. Table 2 summarizes the total number of measured correlations and accidentals for each sample. The total correlations represent the total number of counts (real and accidental) in the entire measurement window. The total accidentals were calculated by integrating an average accidental rate over the entire measurement window. The average accidental window was determined by calculating the average count level for times between 40 and 80 ns. This level will be subtracted out for subsequent comparisons to the Monte Carlo simulations. The relative number of accidentals increases with sample mass and burnup.

In order to observe the trend in (neutron, neutron) correlations versus sample mass the effective ^{240}Pu mass (m_{240}^{eff}) was calculated using the well-known relationship,

$$m_{240}^{eff} = 2.52m_{238} + 1.0m_{240} + 1.68m_{242} \quad (2)$$

where m_{238}, m_{240}, and m_{242} are the masses of ^{238}Pu, ^{240}Pu, and ^{242}Pu in each sample, respectively [8].

Fig. 9 shows a plot of total measured (neutron, neutron) correlations as a function of effective ^{240}Pu mass. A clear increasing trend is observed with increasing mass. Furthermore, the low- and high-burnup samples appear to lie in different regions. This trend is explained by the fact that the (neutron, neutron) correlations are proportional to the (spontaneous plus induced) fission rate. The spontaneous fission rate is in turn proportional to the effective ^{240}Pu mass, whereas the induced fission rate, due to self-multiplication, is related to the content of the (odd-numbered) fissile isotopes, so this second contribution changes when changing the isotopic composition.

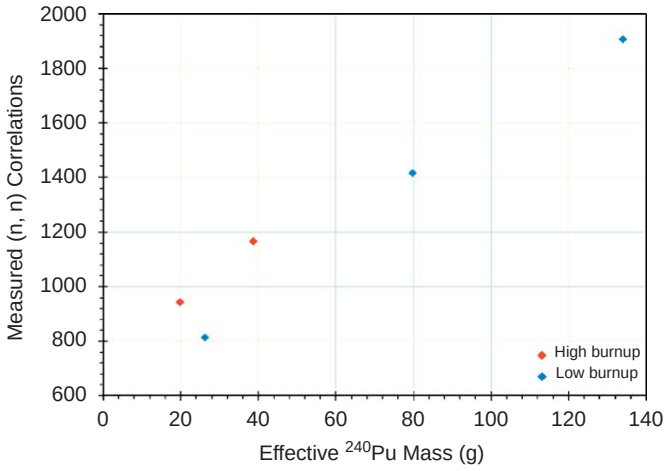

Fig. 9. Total number of measured (neutron, neutron) correlated counts as a function of effective ^{240}Pu mass; results for both low- and high-burnup samples are shown.

4. Monte Carlo analysis

4.1. Description of MCNP-PoliMi

Monte Carlo codes have been widely used to design and analyze measurements such as those considered here; however, when modeling the time-correlated events resulting from gamma-ray interrogation, the widely used Monte Carlo code MCNPX has some limitations. Specifically, MCNPX deviates from physical reality and the particles resulting from fission are not modeled correctly on an event-by-event basis [9]. A modified version of MCNP4C called MCNP-PoliMi has been developed to simulate time-correlated quantities and includes a correlation between individual neutron interactions and corresponding gamma-ray production [10]. MCNP-PoliMi version 1.2.4 is capable of running with all standard MCNP source types and includes several specific spontaneous fission source distributions with correct source multiplicities (i.e., ^{252}Cf, ^{240}Pu, ^{242}Pu, etc.). MCNP-PoliMi also contains angular distributions for fission neutrons that were applied in these calculations. However, there is no correlation between the emitted neutrons and gamma rays. Finally, MCNP-PoliMi also contains distributions for (α, n) reactions for

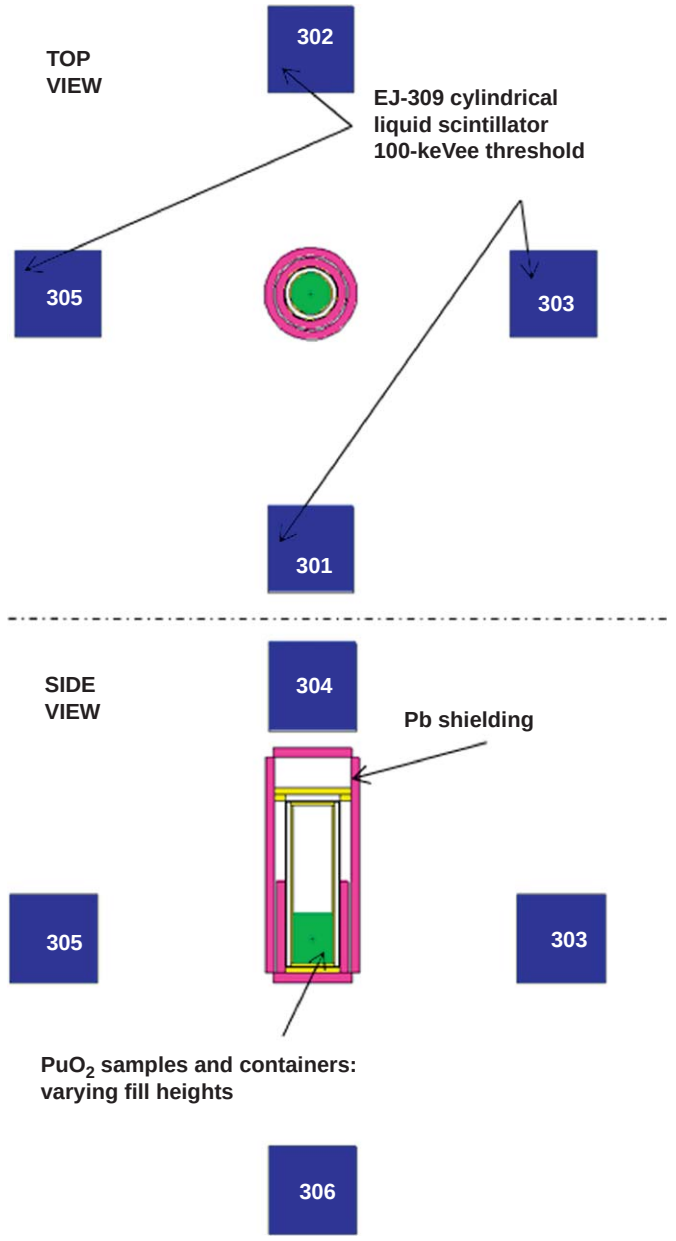

Fig. 10. MCNP-PoliMi model of the PuO_2 sample, container, lead shielding, and EJ-309 scintillation detectors; top and side views are shown.

Table 3
Fraction of spontaneous fission (s.f) and alpha-*n* neutrons emitted from low- and high-burnup PuO_2 samples.

Isotope	Low burnup (%)	High burnup (%)
^{238}Pu(s.f.)	1.43	6.53
^{238}Pu(α, n)	7.39	33.80
^{239}Pu(s.f.)[a]	<0.01	<0.01
^{239}Pu(α, n)	7.49	3.24
^{240}Pu(s.f.)	69.43	37.03
^{240}Pu(α, n)	9.60	5.12
^{241}Pu(s.f.)[a]	<0.001	<0.01
^{241}Pu(α, n)[a]	0.01	0.02
^{242}Pu(s.f.)	4.64	14.23
^{242}Pu(α, n)[a]	0.01	0.02

[a] These contributions were neglected from the MCNP-PoliMi source specification model.

plutonium isotopes in oxides which were utilized in the calculations here.

A post-processing code is then used to load the required data from this file and compute the detector-specific response. In the case of a scintillation detector, the incoming radiation must deposit enough energy to overcome a specific threshold for light output; this threshold is common for neutrons and photons. Different incoming particles interact in different ways: gamma rays interact primarily through Compton scattering on electrons, while neutrons interact through scattering on hydrogen and carbon. The energy deposition in each interaction is converted into light in the post-processor using empirical relationships [11]. The event-by-event interactions modeled in MCNP-PoliMi enables the simulation of detailed detection physics, which is typically disregarded in other simplified code systems. The data given in the MCNP-PoliMi output file makes modeling effects such as varying light outputs of different target nuclei and multiple particle-scattering events possible.

4.2. Description of Monte Carlo model

The MCNP-PoliMi model of the measurement setup included a detailed model of the container with the PuO_2 and surrounding lead sleeves as well as all six EJ-309 scintillators. For simplicity, only the active volume of each scintillator was modeled. Fig. 10 shows the top and side views of the MCNP-PoliMi model.

Each measurement was simulated with the MCNP-PoliMi code. The source for each simulation was modeled using the MCNP-PoliMi internal definitions for plutonium spontaneous fission and neutron production from (α, n) reactions. The relative contributions for each neutron source were computed directly from the isotopic compositions given in Table 1 and the specific activities of each isotope for spontaneous fission and (α, n) in oxides [8]. Table 3 summarizes the fraction of total source neutrons emitted from each reaction for the low- and high-burnup PuO_2 samples. Some contributions were neglected due to their low relative intensity (see Table 3). The small number of ^{238}Pu spontaneous fissions was normalized into the ^{240}Pu and ^{242}Pu energy distributions because a ^{238}Pu spontaneous fission spectrum was unavailable.

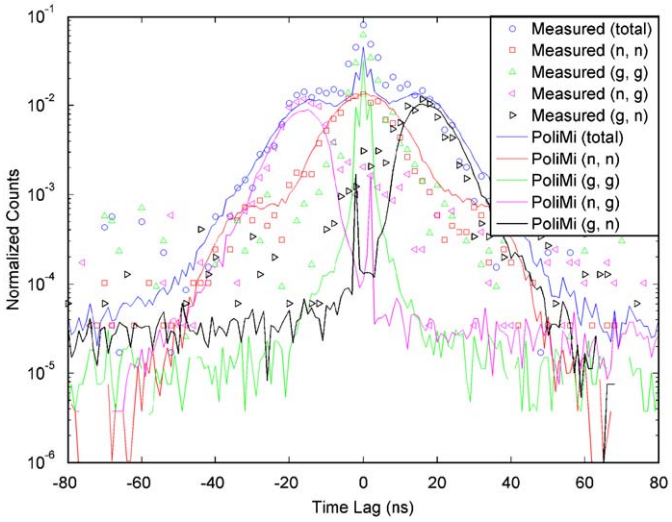

Fig. 11. Comparison of MCNP-PoliMi simulation results to measured data for a 500-g sample of low-burnup PuO_2 powder.

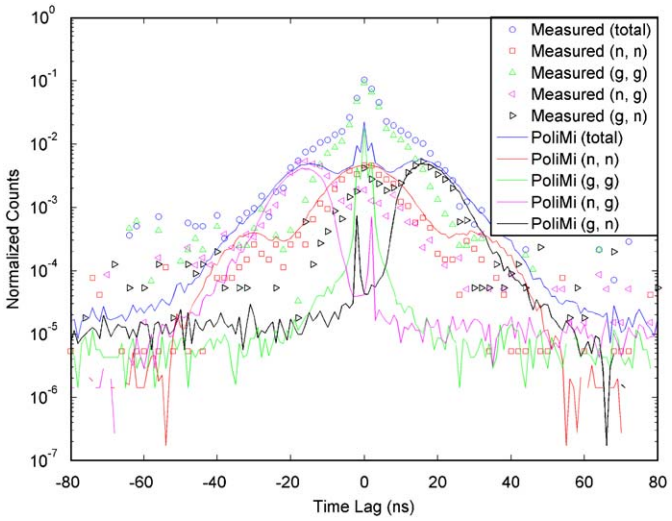

Fig. 12. Comparison of MCNP-PoliMi simulation results to measured data for a 100-g sample of high-burnup PuO_2 powder.

4.3. Simulation results and comparison

The MCNP-PoliMi post-processor was used to compute the time-dependent cross-correlation functions separately for neutrons and gamma rays. The detector deadtime (80 ns) and threshold (100 keVee) were modeled explicitly. The accidental coincidence level of the measured data was subtracted prior to comparison (an average level was computed using time lags between 40 and 80 ns). This effect was not simulated because it required detailed knowledge of the complex background radiation field, which were not available. The data were then normalized to the maximum of the (neutron, neutron) portion of the distribution; all five contributions were normalized to the same factor so the relative magnitudes are preserved.

Figs. 11 and 12 show the comparison of all contributions of the cross-correlation functions for the 500-g, low-burnup sample and the 100-g, high-burnup sample. Good agreement is observed for both cases. As expected, MCNP-PoliMi dramatically underpredicts the gamma-ray contributions for high-burnup sample. This is due to the increased fission product and ^{241}Am buildup that were not modeled. The MCNP-PoliMi model thus neglects fission product decay gamma rays, which would contribute primarily to the (g, g) partial cross-correlation functions.

5. Conclusions

For the first time, measurements of the time-dependent cross-correlation distributions of PuO_2 have been made separately for neutrons and gamma rays. These measurements were performed jointly by the University of Michigan and EURATOM JRC staff on five different samples of varying mass and burnup: 100-, 300- and 500-g low-burnup samples, and 50- and 100-g high-burnup samples. Six EJ-309 liquid scintillation detectors with a digital, offline PSD and pulse timing method were employed to selectively analyze the number of (neutron, neutron) correlations versus plutonium mass. A clear, increasing trend was observed with the low-burnup samples lying along a different line than the high-burnup samples, which proves that a selective analysis of (n, n) correlated counts can be used for quantification of the plutonium in the sample.

Additionally, the measurement scenarios were modeled using the MCNP-PoliMi code. Spontaneous fission and (α, n) source contributions were included and all contributions of the normalized cross-correlation functions were compared. Good agreement was achieved between the measured and simulated data which indicates that the MCNP-PoliMi code has a large potential for modeling time-correlated quantities.

References

[1] S.A. Pozzi, J.T. Mihalczo, P. Peerani, J. Loeschner, L. Cartegni, J.A. Mullens, P. Hausladen, Passive measurements on plutonium oxide samples, in: Proceedings of the Institute of Nuclear Materials Management, 46 Annual Meeting, July 10–14, 2005, Phoenix, Arizona.
[2] S. Guardini, G. Guzzi, F. Mousty, S. Baumann, E. Kuhn, P. de Regge. PERLA: Quality Control Provisions Applied in the Preparation and Characterization of Pu-Bearing Perla Standards, Report EUR 13308 EN, CEC-JRC, Ispra, 1990.
[3] M. Flaska, S.A. Pozzi, Nucl. Instr. and Meth. A 577 (2007) 654.
[4] D. Wolski, M. Moszynski, T. Ludziejewski, A. Johnson, W. Klamra, O. Skeppstedt, Nucl. Instr. and Meth. A 360 (1995) 584.
[5] H. Klein, S. Neumann, Nucl. Instr. and Meth. A 476 (2002) 132.
[6] L.M. Bollinger, G.E. Thomas, Rev. Sci. Instrum. 32 (1961) 1044.
[7] J.B. Birks, The Theory and Practice of Scintillation Counting, Pergamon Press, Oxford, 1964, pp. 219–227.
[8] D. Reilly, N. Ensslin, H. Smith Jr. (Eds.), Passive Nondestructive Assay of Nuclear Materials, Los Alamos National Laboratory Report LA-UR-90-732, 1991.
[9] X-5 Monte Carlo Team. MCNP-A General Monte Carlo N-Particle Transport Code, version 5, vols. 1–3, LA-UR-03-1987, LA-CP-03-0245, and LA-CP-03-0284, Los Alamos National Laboratory, 2003.
[10] S.A. Pozzi, E. Padovani, M. Marseguerra, Nucl. Instr. and Meth. A 513 (2003) 550.
[11] S. Pozzi, E. Padovani, M. Flaska, S. Clarke. MCNP-PoliMi Post-Processing Code, version 1.9, Oak Ridge National Laboratory Internal Report, ORNL/TM-2007/33, 2007.